

AGREEMENT-DRIVEN MULTI-VIEW 3D RECONSTRUCTION FOR LIVE CATTLE WEIGHT ESTIMATION

Rabin Dulal, Wenfeng Jia, Lihong Zheng, Jane Quinn

Charles Sturt University

ABSTRACT

Accurate cattle live weight estimation is vital for livestock management, welfare, and productivity. Traditional methods, such as manual weighing using a walk-over weighing system or proximate measurements using body condition scoring, involve manual handling of stock and can impact productivity from both a stock and economic perspective. To address these issues, this study investigated a cost-effective, non-contact method for live weight calculation in cattle using 3D reconstruction. The proposed pipeline utilized multi-view RGB images with SAM 3D-based agreement-guided fusion, followed by ensemble regression. Our approach generates a single 3D point cloud per animal and compares classical ensemble models with deep learning models under low-data conditions. Results show that SAM 3D with multi-view agreement fusion outperforms other 3D generation methods, while classical ensemble models provide the most consistent performance for practical farm scenarios ($R^2 = 0.69 \pm 0.10$, MAPE = $2.22 \pm 0.56\%$), making this practical for on-farm implementation. These findings demonstrate that improving reconstruction quality is more critical than increasing model complexity for scalable deployment on farms where producing a large volume of 3D data is challenging.

Index Terms— 3D cattle reconstruction, weight estimation, machine learning, ensemble, deep learning, point cloud.

1. INTRODUCTION

Live weight is a key metric of livestock performance in both beef and sheep production systems. As livestock systems face increasing sustainability challenges, accurate information on live weight gain is needed to guide management decisions, but preferably without impacting animal performance to achieve that measure. Currently, there is no reliable substitution for manual weighing of stock, as visual scoring systems can be imprecise, whilst also frequently requiring hands-on assessment that can impact live weight gain through handling.

Currently, live weight measurement of cattle is typically performed using direct methods, such as measurement using walk-over weighing scales placed in a crush or chute, or through indirect methods based on cattle morphology and physical presentation [1]. Although direct weighing is

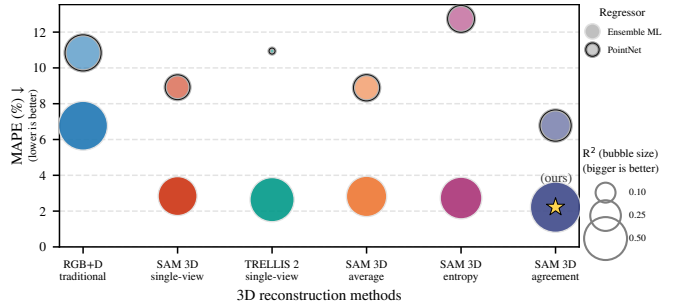


Fig. 1: MAPE and R^2 of weight estimation across 3D cattle reconstruction methods.

accurate, manual body measurements and direct weighing are time-consuming, labour-intensive, costly, and require restraining cattle, which induces stress, reduces productivity, and poses safety risks to both producer and animal alike [2, 3]. Consequently, recent studies [2, 4, 5, 6, 7, 8, 9, 10, 11] have explored non-contact weight estimation using low-cost sensors and machine vision, enabling faster, safer, and less invasive weight prediction than scale-based methods.

In recent years, machine learning (ML) and deep learning (DL) approaches have been increasingly adopted for live weight prediction based on animal morphological characteristics. These methods offer a strong capability to model complex and non-linear relationships between body shape and weight from the data.

3D data methodologies have gained increasing prominence for live weight estimation due to their ability to capture comprehensive spatial and volumetric information that cannot be reliably obtained from 2D images [5]. Unlike 2D vision systems, which are sensitive to viewpoint, lighting conditions, and occlusion, 3D sensing technologies provide accurate depth measurements and geometric representations of the animal's body structure [6]. This enables more precise estimation of body volume, surface area, and shape-related features that are strongly correlated with live weight [12]. Consequently, 3D vision-based approaches offer improved robustness and generalization, particularly in unconstrained farm environments, making them well-suited for non-contact, automated, and accurate livestock weight prediction [4].

Recent studies on non-contact cattle weight estimation have used 3D data acquired from stereo camera systems, Li-

DAR sensors, and / or depth cameras such as Kinect and Intel RealSense to generate point clouds or 3D meshes of cattle body shape, size and condition [4, 7, 8, 9]. Weight prediction is typically performed using either classical ML models applied to handcrafted 3D features or DL methods that directly learn from 3D representations [5, 6, 10, 13]. Tab. 1 summarises existing non-contact live weight estimation studies.

Table 1: Summary of non-contact animal live weight estimation studies. Our method achieves 3D reconstruction using only RGB images, with *no need* for extra sensing hardware (Depth/LiDAR/Stereo).

Ref.	Data/animal	Animal	Weight Model	RGB	Depth info	Metrics
[2]	11	Cattle	MRGBDM	✓	✓	MAE, MAPE
[4]	21	Cattle	PointNet++	✗	✓	MAPE, RMSE
[5]	5	Pig	PointNet	✓	✓	R^2 , RMSE
[6]	5	Chicken	PointNet++	✓	✓	MAE, MAPE
[7]	50	Pig	MACNN	✓	✓	MAE, MAPE, RMSE
[8]	14	Pig	DNN	✓	✓	R^2 , MAE
[9]	4	Cattle	RF	✗	✓	MAE, MAPE
[10]	5	Pig	LR	✗	✓	MAPE
[11]	4	Pig	ANN	✓	✓	MAE, RMSE
Ours	1	Cattle	Ensemble ML	✓	✗(No need)	R^2 , MAPE, MAE

The existing practical use of 3D-based live cattle weight estimation is limited by cattle movement, high hardware costs, complex installation and calibration, and the need for technical expertise, while DL methods further require large, well-labelled datasets that are difficult to obtain in real farm environments [14, 15].

To address these challenges, this study makes three key contributions: **(i)** it proposes a cost-effective, non-contact pipeline that reconstructs accurate 3D representations from RGB images without requiring expensive sensors or preprocessing; **(ii)** it introduces an agreement-driven fusion strategy for SAM 3D-based multi-view 3D reconstruction to obtain a reliable and consistent 3D representation; and **(iii)** it develops an ensemble regression framework for cattle weight estimation that effectively leverages geometric features extracted from the reconstructed 3D models.

2. METHODOLOGY

Building on recent advances in 3D reconstruction [16, 17, 18], we propose a non-contact pipeline that reconstructs accurate 3D representations of live cattle from RGB images and estimates their weight.

The overall pipeline is illustrated in Fig. 2. **First**, the dataset [19] is collected using cameras, and masks are generated by SAM3 [20] with a text prompt. **Second**, given the images and masks, 3D reconstruction is performed by SAM 3D with agreement fusion; we also reconstruct 3D live cattle using other methods, including conventional RGB+D [19] and TRELLIS2 [17] etc., and compare these approaches through downstream live weight-estimation performance. **Finally**, cattle live weight is estimated using ensemble learning.

2.1. Dataset Source Description

The dataset used in this study is publicly available [19] and contains **103**×**3** live cattle RGB images captured from left, right, and top views, along with corresponding 3D point clouds and live cattle weights. The point clouds include surrounding walls and floors, which were removed by us using RANSAC [21] to obtain clean representations.

2.2. 3D Data Generation

SAM 3D [16] is a two-stage generative foundation model for single-image 3D reconstruction, introduced in 2025. Its strong modeling capability enables the reconstruction of accurate 3D Gaussian point clouds from only RGB images, which in turn supports downstream tasks such as cattle weight estimation. However, SAM 3D originally supports only single-view image input. In contrast, [18] extends SAM 3D to the multi-view setting by introducing simple average fusion and entropy-based fusion, thereby enabling multi-view 3D reconstruction based on SAM 3D.

Inspired by [18], we introduce an agreement-weighted multi-view fusion strategy that operates within SAM 3D’s iterative latent generation. The inputs are V masked views $\{(I^{(v)}, M^{(v)})\}_{v=1}^V$ (RGB + mask only). Each view is encoded into a conditioning representation:

$$\mathbf{c}^{(v)} = E(I^{(v)}, M^{(v)}), \quad v = 1, \dots, V, \quad (1)$$

where $E(\cdot)$ denotes the SAM 3D’s encoder and $\mathbf{c}^{(v)}$ are view-specific conditioning tokens.

Let \mathbf{x}_t denote the current latent state at step t . Conditioned on each view, the stage-specific transformers predict a view-dependent latent update:

$$\mathbf{u}_t^{(v)} = f_\theta(\mathbf{x}_t, t; \mathbf{c}^{(v)}), \quad v = 1, \dots, V. \quad (2)$$

The agreement weights are computed and fused $\{\mathbf{u}_t^{(v)}\}$ before advancing the latent state. Specifically, for each latent location ℓ , we first form a multi-view consensus center (mean center) using the per-view update vectors: $\mathbf{u}_{t,\ell}^{(v)} \in \mathbb{R}^D$:

$$\mathbf{m}_{t,\ell} = \text{Center}\left(\{\mathbf{u}_{t,\ell}^{(j)}\}_{j=1}^V\right). \quad (3)$$

Then, measuring how much each view deviates from this consensus via an RMS distance:

$$d_{t,\ell}^{(v)} = \sqrt{\frac{1}{D} \left\| \mathbf{u}_{t,\ell}^{(v)} - \mathbf{m}_{t,\ell} \right\|_2^2 + \varepsilon}, \quad (4)$$

where D is the latent channel dimension and ε is a small constant for numerical stability. After that, converting deviations into an unnormalized agreement score:

$$\text{agreement}_{t,\ell}^{(v)} = \exp\left(-\beta d_{t,\ell}^{(v)}\right), \quad (5)$$

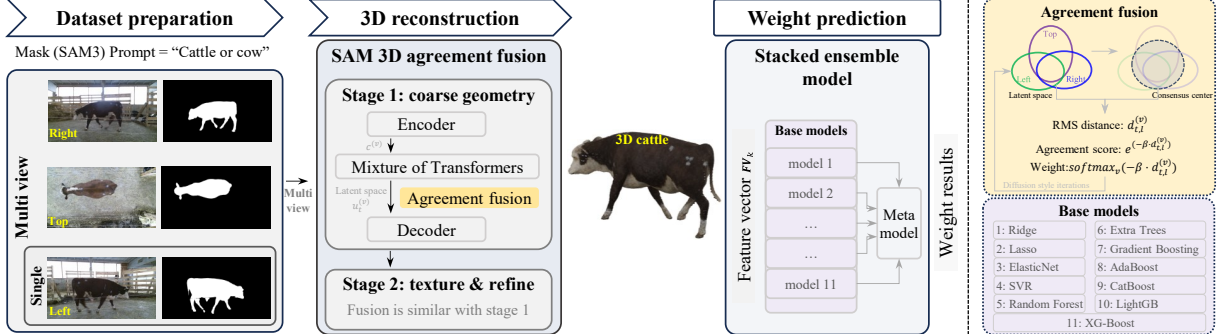


Fig. 2: Pipeline of agreement-driven multi-view 3D reconstruction for non-contact live cattle weight estimation.

And apply a softmax over views to obtain fusion weights:

$$w_{t,\ell}^{(v)} = \frac{agreement_{t,\ell}^{(v)}}{\sum_{j=1}^V agreement_{t,\ell}^{(j)}} = \text{softmax}_v(-\beta d_{t,\ell}^{(v)}), \quad (6)$$

$$\bar{\mathbf{u}}_{t,\ell} = \sum_{v=1}^V w_{t,\ell}^{(v)} \mathbf{u}_{t,\ell}^{(v)}. \quad (7)$$

Here β controls the sharpness of view selection. The fused update $\bar{\mathbf{u}}_t$ is then used by the sampler to advance the latent state, producing Stage 1 and, analogously, the refined Stage 2 for decoding into 3D outputs.

2.3. Weight Prediction

In this study, live cattle weight is estimated from 3D point clouds using feature extraction, multiple regression models, and a stacked ensemble approach. Let the 3D point cloud of the k -th cattle be denoted by \mathbf{P}_k , defined as

$$\mathbf{P}_k = \{\mathbf{p}_{k,n} = (x_{k,n}, y_{k,n}, z_{k,n}) \in \mathbb{R}^3\}_{n=1}^{N_k},$$

where $k = 1, 2, \dots, K$ indexes the cattle instances, $n = 1, 2, \dots, N_k$ indexes the points within the k -th point cloud, and N_k denotes the total number of points in \mathbf{P}_k .

For each cattle, a feature vector \mathbf{FV}_k is computed to capture geometric, statistical, and density-based properties. These features include geometric descriptors (length, width, height, bounding box and convex hull volumes, and surface area), shape descriptors, spatial distribution (percentiles along the x , y , and z axes), density and statistical moments (Z-axis densities in three vertical sections and mean and standard deviation along each axis). The feature selection is motivated by existing studies [9, 10, 12, 19], which demonstrate the effectiveness of global body dimensions, shape descriptors, spatial distribution, and statistical moments for cattle weight estimation. These features are combined into a unified representation to capture both geometric structure and statistical characteristics.

$$\begin{aligned} \mathbf{FV}_k &\triangleq [\mathbf{F}_k^{(g)}, \mathbf{F}_k^{(a)}, \mathbf{F}_k^{(q_x)}, \mathbf{F}_k^{(q_y)}, \mathbf{F}_k^{(q_z)}, \mathbf{F}_k^{(\rho)}, \mathbf{F}_k^{(\mu)}], \\ \mathcal{P} &\triangleq \{10, 25, 50, 75, 90\}, \\ \mathbf{F}_k^{(g)} &\triangleq [l, w, h, V_{\text{bbox}}, V_{\text{hull}}, A_{\text{surface}}]^\top, \\ \mathbf{F}_k^{(a)} &\triangleq [\lambda_1/\lambda_2, \lambda_2/\lambda_3]^\top, \\ \mathbf{F}_k^{(q_x)} &\triangleq [x_p]_{p \in \mathcal{P}}^\top, \quad \mathbf{F}_k^{(q_y)} \triangleq [y_p]_{p \in \mathcal{P}}^\top, \quad \mathbf{F}_k^{(q_z)} \triangleq [z_p]_{p \in \mathcal{P}}^\top, \\ \mathbf{F}_k^{(\rho)} &\triangleq [\rho_{z1}, \rho_{z2}, \rho_{z3}]^\top, \\ \mathbf{F}_k^{(\mu)} &\triangleq [\mu_x, \sigma_x, \mu_y, \sigma_y, \mu_z, \sigma_z]^\top \end{aligned} \quad (8)$$

The resulting feature matrix $FV \in \mathbb{R}^{1 \times d}$ and target vector $T_{\text{target}} \in \mathbb{R}$ (live weight in kg) are used to train a set of 11 base regression models,

$$\mathcal{G} = \{g_m : \mathbb{R}^{1 \times d} \rightarrow \mathbb{R} \mid m = 1, \dots, 11\} \quad (9)$$

These models cover linear, kernel-based, and ensemble learning paradigms, enabling a robust evaluation of the relationship between 3D morphological features and cattle live weight. The regressors include Linear Regression, Ridge, Lasso, ElasticNet, SVR, Random Forest, Extra Trees, Gradient Boosting, AdaBoost, CatBoost, LightGBM, and XG-Boost. For the k -th sample, the prediction of the m -th base model is $\hat{T}_{\text{target},k,m} = f_m(\mathbf{FV}_k)$.

To leverage complementary model strengths, a stacked ensemble is constructed. Let the predictions of the top m_{top} base models for the k -th sample be:

$$\hat{T}_{\text{target},k}^{\text{base}} = [\hat{T}_{\text{target},k,1}, \dots, \hat{T}_{\text{target},k,m_{\text{top}}}]^\top \quad (10)$$

A Ridge regression model serves as the self-learner and produces the final prediction.

$$\hat{T}_{\text{target},k}^{\text{final}} = g(\hat{T}_{\text{target},k}^{\text{base}}) = \mathbf{w}_{\text{self}}^\top \hat{T}_{\text{target},k}^{\text{base}} + b_{\text{self}} \quad (11)$$

where \mathbf{w}_{self} and b_{self} are learned by minimizing the Ridge-regularized squared error,

$$\min_{\mathbf{w}_{\text{self}}} \sum_{k=1}^n (\hat{T}_{\text{target},k} - \hat{T}_{\text{target},k}^{\text{final}})^2 + \alpha \|\mathbf{w}_{\text{self}}\|_2^2 \quad (12)$$

with α fixed to 1.0 to provide stable $L2$ regularization under limited training data. The proposed methodology is evaluated using 5-fold cross-validation, and performance is assessed using the coefficient of determination (R^2), mean absolute error (MAE), and mean absolute percentage error (MAPE).

3. RESULTS AND DISCUSSION

3.1. 3D Cattle Body Reconstruction

As the agreement-based fusion proceeds (Sec. 2.2), the reconstructed live cattle model becomes progressively more robust and complete. Fig. 3 visualizes the evolution of the agreement scores defined in Eq. 5 across diffusion steps t during the coarse Stage 1. Fig. 3 (a)–(f) shows the spatial distribution of the mean multi-view $agreement_{t,\ell}$ for different cattle parts in the Stage 1 latent space as the iterations progress (t). Fig. 3 (g) plots the per-view mean agreement score over diffusion steps. The agreement rises rapidly and approaches 1 at around $t \approx 40$, indicating that $d_{t,\ell}^{(v)}$ in Eq. 5 quickly decreases towards 0; consequently, all views strongly align with the consensus center $\mathbf{m}_{t,\ell}$ in latent space.

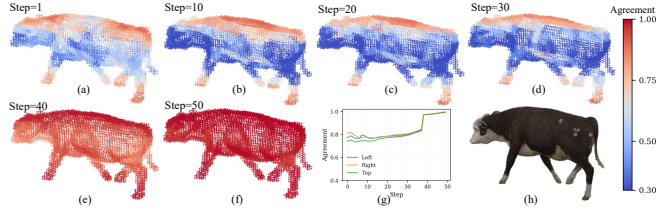


Fig. 3: Visualization of multi-view agreement fusion in SAM 3D coarse geometry stage latent space. (a)–(f) shows the spatial distribution of the mean 3-view agreement score as the iterations progress. (g) is the per-view mean agreement score. (h) is the visualization of the final multi-view fused 3D Gaussian point cloud.

As presented in Fig. 4, it visually compares different methods used for 3D reconstruction. Among these methods, RGB+D reconstruction yields the most natural cattle shape, while details are coarse, edges are blurry, and occlusions noticeably degrade the results. Among DL methods, TRELLIS2 achieves the best visual quality but is highly sensitive to occlusions. Moreover, for SAM 3D-based approaches, multi-view agreement fusion performs best overall, producing more consistent cattle shapes with fewer artifacts.

3.2. Cattle Weight Regression

18 ML models and 2 DL models were evaluated. The ensemble of the top 11 ML models achieved the best performance, as including additional models beyond the top 11 did not yield significant improvement, as shown in Fig. 5. Notably, weight estimates from DL-based 3D reconstructions significantly outperform those obtained using conventional RGB+D methods. Detailed results are provided in the Supplementary Material.

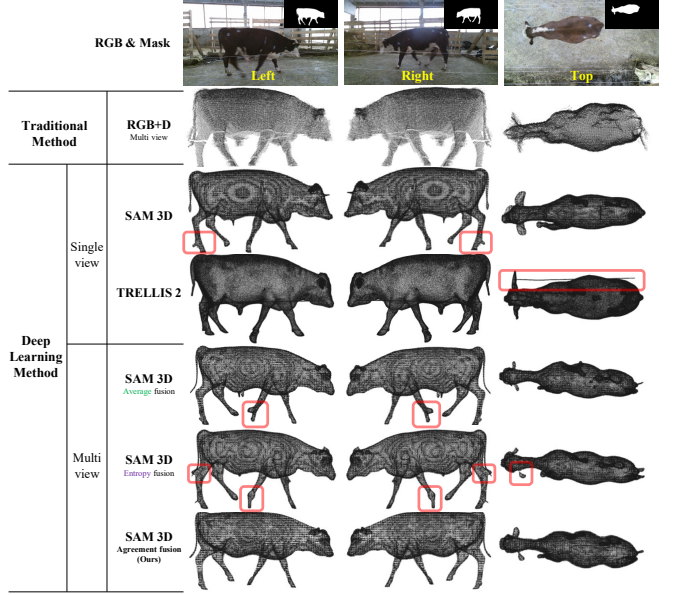


Fig. 4: Visual Comparison of different point clouds. Obvious structural anomalies are marked with red boxes. SAM 3D outputs Gaussian point clouds; however, we ignore the Gaussian parameters and visualise them as uncoloured point clouds for comparison.

Tab. 2 presents the results of cattle weight prediction using the ensemble model, PointNet and PointNet++. Classical ensemble models consistently outperform DL models (PointNet and PointNet++) on different cattle point cloud datasets. The ensemble model trained on **SAM 3D with agreement fusion** dataset achieves the highest R^2 of 0.69 ± 0.10 , the best MAE of 9.16 ± 2.32 kg, and MAPE of $2.22 \pm 0.56\%$. These results demonstrate that SAM 3D-based multi-view reconstruction with agreement fusion produces the most accurate and reliable 3D representations, while classical ensemble models outperform DL approaches in low-data scenarios.

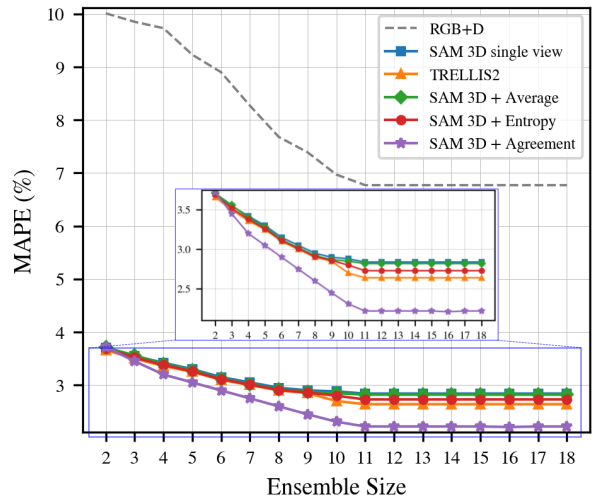


Fig. 5: Effect of ensemble size on MAPE (%) for different 3D datasets. Performance improves with increasing top ML models but stabilizes after Top-11 for both RGB+D and DL-based 3D methods.

An ensemble of classical ML models consistently outperforms DL models across all 3D reconstruction methods, as shown in Tab. 2 and Fig. 6. On conventional RGB+D datasets, the ensemble regressor attains an R^2 of 0.65 ± 0.09 , outperforming PointNet (0.35 ± 0.12) and PointNet++. In the other datasets, in terms of MAE and MAPE, it also shows that ensemble ML clearly outperforms the DL models. This underperformance stems primarily from the scarcity of training data: each cattle has only one point cloud, which is insufficient for deep networks to learn meaningful 3D spatial patterns, leading to overfitting and poor generalization.

Table 2: Regression results on point clouds using 5-fold cross-validation (mean \pm std). This table reports only Ensemble ML, PointNet, PointNet++. The best 3D reconstruction method is marked in red, the second best is marked in blue; full results are provided in the supplementary material.

Method	Ensemble ML	PointNet	PointNet++
R^2 (\uparrow)			
RGB+D	0.65 ± 0.09	0.35 ± 0.12	0.39 ± 0.11
SAM 3D single view	0.41 ± 0.11	0.16 ± 0.10	0.21 ± 0.11
TRELLIS2	0.53 ± 0.15	-0.41 ± 0.18	0.07 ± 0.03
SAM 3D + average	0.44 ± 0.14	0.18 ± 0.09	0.23 ± 0.10
SAM 3D + entropy	0.47 ± 0.08	0.19 ± 0.08	0.24 ± 0.09
SAM 3D + agreement	0.69 ± 0.10	0.26 ± 0.09	0.30 ± 0.08
MAE (kg, \downarrow)			
RGB+D	29.51 ± 6.67	48.5 ± 11.5	58.8 ± 20.2
SAM 3D single view	11.83 ± 2.04	39.9 ± 6.5	47.6 ± 15.2
TRELLIS2	11.12 ± 2.68	48.9 ± 35.3	40.8 ± 12.0
SAM 3D + average	11.77 ± 2.21	39.7 ± 1.7	47.5 ± 1.6
SAM 3D + entropy	11.38 ± 1.21	56.9 ± 15.2	51.3 ± 5.9
SAM 3D + agreement	9.16 ± 2.32	30.3 ± 1.7	35.9 ± 6.0
MAPE (% , \downarrow)			
RGB+D	6.77 ± 1.46	10.84 ± 2.59	13.16 ± 4.52
SAM 3D single view	2.84 ± 0.49	8.92 ± 1.45	10.66 ± 3.41
TRELLIS2	2.64 ± 0.64	10.94 ± 7.89	9.12 ± 2.90
SAM 3D + average	2.82 ± 0.53	8.89 ± 0.38	10.62 ± 0.35
SAM 3D + entropy	2.73 ± 0.29	12.74 ± 3.40	11.48 ± 1.31
SAM 3D + agreement	2.22 ± 0.56	6.78 ± 0.38	8.02 ± 1.34

As illustrated in Tab. 2 and Fig. 1, DL-based cattle 3D reconstruction methods substantially outperform conventional RGB+D approaches. Across the considered 3D reconstruction methods, SAM 3D-based multi-view agreement fusion provides the most informative 3D representation for weight prediction, consistently improving MAE, MAPE and R^2 . Notably, in terms of R^2 , agreement fusion (0.69 ± 0.10) is the only method that surpasses the conventional RGB+D baseline (0.65 ± 0.09). The remaining DL-based 3D methods achieve lower R^2 values. This suggests that agreement fusion provides not only higher reconstruction quality but also stronger stability for downstream weight estimation.

In terms of MAE and MAPE, Tab. 2 and Fig. 6(b, c) show that SAM 3D with multi-view agreement fusion dataset provides the best performance. Among the SAM 3D-based multi-view reconstruction variants, only agreement fusion achieves a clear improvement in weight estimation over single-view SAM 3D. However, the gain

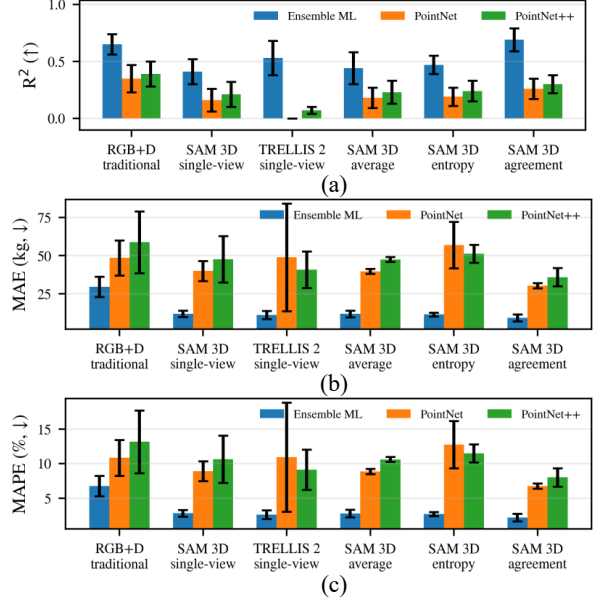


Fig. 6: Comparison of weight estimation performance across models and 3D reconstruction methods. (a) results of R^2 ; (b) results of MAE; (c) results of MAPE.

from the conventional RGB+D baseline ($MAE=29.51 \pm 6.67$, $MAPE=6.77 \pm 1.46$) to SAM 3D is much larger than the additional gain from single-view SAM 3D to multi-view agreement fusion ($MAE=9.16 \pm 2.32$, $MAPE=2.22 \pm 0.56$). Even so, the higher R^2 achieved by the agreement fusion method ($R^2=0.69 \pm 0.10$) suggests markedly greater reliability for practical cattle weight estimation in real applications.

4. CONCLUSION

This study presented a cost-effective, non-contact pipeline for live weight estimation from RGB images. Specifically, we developed a multi-view 3D reconstruction model that extends SAM 3D via a novel agreement fusion strategy. Notably, our results demonstrate that agreement fusion robustly utilizes cross-view information, leading to significant gains in reconstruction accuracy and reliability. Furthermore, the results confirmed that DL-based 3D reconstruction methods produce superior representation for live weight estimation compared to conventional RGB+D methods. Regarding the live weight estimation, the ensemble learning model, combining 11 ML models, was found to estimate live weights more accurately than DL model in low-data scenarios.

Overall, the proposed pipeline significantly reduces the time, cost, manpower, and effort required to generate 3D models. Consequently, it offers a robust solution for accurate individual animal live weight estimation, which is highly suitable for practical deployment in real world livestock management situations.

SUPPLEMENTARY MATERIAL

5. SELECTION CRITERIA OF ML MODELS

For effective weight prediction, 18 regression models were used in this study. These include Extra Trees [22], Random Forest [23], AdaBoost [24], Gradient Boosting [25], XGBoost [26], CatBoost [27], LightGBM [28], Linear Regression [29], Ridge [30], Lasso [31], Elastic Net [32], Support Vector Regression (SVR) [33], Nu-Support Vector Regression (NuSVR) [34], Decision Tree [35], k-Nearest Neighbors (KNN) [36], Huber Regression [37], RANSAC [21], and Ridge Regression [38].

All regression models were trained using the original point cloud data (RGB+D) to identify and rank them from best to worst, as summarized in Table 3. To evaluate the benefits of ensembling, results for all models are also presented in Table 4.

Table 3: Performance comparison of regression models on original point cloud data (RGB+D), ranked by MAPE (%).

Rank	Model	R^2	MAE (kg)	MAPE (%)
1	ExtraTrees	0.3044	47.20	10.57
2	RandomForest	0.2585	48.20	10.82
3	AdaBoost	0.2603	50.01	11.21
4	XGBoost	0.1756	50.60	11.31
5	GradientBoosting	0.2091	50.70	11.32
6	CatBoost	0.1800	52.10	11.64
7	Ridge	0.2028	53.60	12.00
8	LightGBM	0.0100	54.90	12.27
9	Lasso	0.1108	55.50	12.41
10	ElasticNet	0.0781	56.50	12.63
11	SVR	-0.0442	60.01	13.40
12	Linear Regression	-0.2089	61.03	13.89
13	NuSVR	-0.0534	64.61	14.51
14	DecisionTree	-0.5813	65.12	14.62
15	Huber	0.1070	67.40	15.00
16	KNN	-0.1140	69.48	15.25
17	BayesianRidge	-0.1136	69.70	15.47
18	RANSAC	-7.1467	134.91	31.81

The results of the ensemble of top 2 to top 18 models are as presented in Table 4.

The results show that after ensembling top 11 models, the performance does not gain significantly, and there is no value added in the performance by adding more than 11 models.

6. CATTLE WEIGHT REGRESSION

The results of cattle weight prediction are presented in Table 5. The table shows that the ensemble of the 11 top-performing regression models consistently outperforms the individual models. Moreover, the 3D point cloud generated using SAM-based multi-view reconstruction with agreement fusion achieves the best reconstruction quality, which is reflected in the most accurate weight prediction results.

Table 4: Performance of ensemble models formed by progressively adding top-ranked regressors on RGB+D data.

Ensemble Size	R^2	MAE (kg)	MAPE (%)
Top2	0.3200	46.70	10.01
Top3	0.3783	41.32	9.85
Top4	0.3862	40.75	9.73
Top5	0.5300	40.42	9.23
Top6	0.5500	37.88	8.90
Top7	0.5510	35.69	8.27
Top8	0.5928	33.18	7.68
Top9	0.6100	32.07	7.39
Top10	0.6500	30.35	6.97
Top11	0.6500	29.51	6.77
Top12	0.6481	29.48	6.77
Top13	0.6571	30.01	6.77
Top14	0.6439	29.91	6.77
Top15	0.6550	29.16	6.77
Top16	0.6491	29.06	6.77
Top17	0.6473	29.96	6.77
Top18	0.6498	29.43	6.77

7. REFERENCES

- [1] Zhuoyi Wang, Saeed Shadpour, Esther Chan, Vanessa Rotondo, Katharine M Wood, and Dan Tulpan, “Asas-nanp symposium: Applications of machine learning for livestock body weight prediction from digital images,” *Journal of animal science*, 2021.
- [2] Alexey Ruchay, Vitaly Kober, Konstantin Dorofeev, Vladimir Kolpakov, Alexey Gladkov, and Hao Guo, “Live weight prediction of cattle based on deep regression of rgb-d images,” *Agriculture*, 2022.
- [3] Alexey Ruchay, Vitaly Kober, Konstantin Dorofeev, Vladimir Kolpakov, Kinispay Dzhulamanov, Vsevolod Kalschikov, and Hao Guo, “Comparative analysis of machine learning algorithms for predicting live weight of hereford cows,” *Computers and Electronics in Agriculture*, 2022.
- [4] Zixia Hou, Lyuwen Huang, Qi Zhang, and Yuanshuang Miao, “Body weight estimation of beef cattle with 3d deep learning model: Pointnet++,” *Computers and Electronics in Agriculture*, 2023.
- [5] Shiva Paudel, Rafael Vieira de Sousa, Sudhendu Raj Sharma, and Tami Brown-Brandl, “Deep learning models to predict finishing pig weight using point clouds,” *Animals*, 2023.
- [6] Haikun Zheng, Chuang Ma, Dong Liu, Junduan Huang, Ruitian Chen, Cheng Fang, Jikang Yang, Daniel Berckmans, Tomas Norton, and Tiemin Zhang, “Weight prediction method for individual live chickens based on single-view point cloud information,” *Computers and Electronics in Agriculture*, 2025.
- [7] Yao Liu, Jie Zhou, Yifan Bian, Taishan Wang, Hongxiang Xue, and Longshen Liu, “Estimation of weight and

Table 5: Performance comparison of regression models on point cloud data using 5-fold cross-validation (mean \pm SD).

Metric / Model	ExtraTrees	RF	AdaBoost	GB	Ridge	CatBoost	XGBoost	Lasso	ElasticNet	LightGBM	SVR	PointNet	PointNet++	Ensemble
Original point cloud														
R^2	0.30 \pm 0.13	0.26 \pm 0.11	0.26 \pm 0.11	0.21 \pm 0.15	0.20 \pm 0.12	0.18 \pm 0.14	0.18 \pm 0.17	0.11 \pm 0.13	0.08 \pm 0.10	0.01 \pm 0.18	-0.04 \pm 0.03	0.35 \pm 0.12	0.39 \pm 0.11	0.65 \pm 0.09
MAE (kg)	47.20 \pm 13.80	48.20 \pm 14.00	50.00 \pm 15.20	50.70 \pm 14.10	53.60 \pm 20.30	52.10 \pm 16.00	50.60 \pm 14.10	55.50 \pm 17.10	56.50 \pm 16.10	54.90 \pm 13.50	60.10 \pm 19.70	48.50 \pm 11.50	58.80 \pm 20.20	29.51 \pm 6.67
MAPE (%)	10.57 \pm 3.18	10.82 \pm 3.26	11.21 \pm 3.52	11.32 \pm 3.14	12.00 \pm 4.54	11.64 \pm 3.57	11.31 \pm 3.15	12.41 \pm 4.63	12.63 \pm 4.28	12.27 \pm 3.02	13.40 \pm 4.39	10.84 \pm 2.59	13.16 \pm 4.52	6.77 \pm 1.46
SAM multiview + agreement fusion														
R^2	0.25 \pm 0.25	0.22 \pm 0.24	0.21 \pm 0.27	0.49 \pm 0.45	0.02 \pm 0.15	0.41 \pm 0.44	0.32 \pm 0.24	0.02 \pm 0.09	0.02 \pm 0.05	-0.46 \pm 0.37	-0.08 \pm 0.09	0.26 \pm 0.09	0.30 \pm 0.08	0.69 \pm 0.10
MAE (kg)	18.00 \pm 2.20	17.90 \pm 1.50	18.60 \pm 1.80	20.80 \pm 2.80	16.80 \pm 2.10	19.90 \pm 2.40	19.50 \pm 2.40	17.20 \pm 1.80	17.50 \pm 1.80	20.50 \pm 1.80	16.50 \pm 1.60	30.30 \pm 1.70	35.90 \pm 6.00	9.16 \pm 2.32
MAPE (%)	4.25 \pm 0.52	4.20 \pm 0.36	4.17 \pm 0.34	4.66 \pm 0.61	3.76 \pm 0.47	4.45 \pm 0.50	4.44 \pm 0.56	3.83 \pm 0.42	3.90 \pm 0.41	4.58 \pm 0.36	3.73 \pm 0.36	6.78 \pm 0.38	8.02 \pm 1.34	2.22 \pm 0.56
SAM Singl View														
R^2	0.12 \pm 0.21	0.09 \pm 0.14	0.07 \pm 0.16	0.04 \pm 0.14	0.10 \pm 0.09	0.17 \pm 0.16	0.20 \pm 0.16	0.05 \pm 0.05	0.04 \pm 0.04	-0.08 \pm 0.09	-0.08 \pm 0.09	0.16 \pm 0.10	0.21 \pm 0.11	0.41 \pm 0.11
MAE (kg)	18.60 \pm 3.60	18.30 \pm 2.80	17.90 \pm 2.70	20.70 \pm 2.80	17.60 \pm 2.40	19.10 \pm 2.90	20.20 \pm 2.10	18.30 \pm 2.00	18.30 \pm 1.90	19.00 \pm 2.80	16.80 \pm 1.60	39.90 \pm 6.50	47.60 \pm 15.20	11.83 \pm 2.04
MAPE (%)	4.16 \pm 0.81	4.06 \pm 0.66	4.00 \pm 0.63	4.63 \pm 0.63	3.96 \pm 0.55	4.27 \pm 0.67	4.51 \pm 0.43	3.95 \pm 0.47	3.95 \pm 0.44	4.26 \pm 0.65	3.74 \pm 0.36	8.92 \pm 1.45	10.66 \pm 3.41	2.84 \pm 0.49
SAM + average fusion														
R^2	0.22 \pm 0.22	0.28 \pm 0.26	0.26 \pm 0.23	0.27 \pm 0.16	0.06 \pm 0.05	0.22 \pm 0.11	0.26 \pm 0.13	0.04 \pm 0.04	0.04 \pm 0.04	-0.58 \pm 0.50	-0.09 \pm 0.09	0.18 \pm 0.09	0.23 \pm 0.10	0.44 \pm 0.14
MAE (kg)	19.10 \pm 2.30	19.30 \pm 1.90	19.10 \pm 2.30	22.80 \pm 2.10	17.60 \pm 1.70	19.00 \pm 2.00	22.80 \pm 3.40	18.60 \pm 1.80	18.60 \pm 1.80	21.30 \pm 3.30	16.70 \pm 1.50	39.70 \pm 1.70	47.50 \pm 1.60	11.77 \pm 2.21
MAPE (%)	4.26 \pm 0.51	4.32 \pm 0.42	4.30 \pm 0.50	5.08 \pm 0.48	3.95 \pm 0.41	4.24 \pm 0.45	4.93 \pm 0.70	3.98 \pm 0.41	3.97 \pm 0.41	4.77 \pm 0.72	3.74 \pm 0.35	8.89 \pm 0.38	10.62 \pm 0.35	2.82 \pm 0.53
SAM + entropy fusion														
R^2	0.09 \pm 0.18	0.12 \pm 0.12	0.22 \pm 0.12	0.33 \pm 0.21	0.01 \pm 0.08	0.11 \pm 0.11	0.15 \pm 0.09	0.01 \pm 0.05	0.02 \pm 0.04	-0.17 \pm 0.21	-0.08 \pm 0.09	0.19 \pm 0.08	0.24 \pm 0.09	0.47 \pm 0.08
MAE (kg)	17.50 \pm 0.70	17.60 \pm 0.90	18.20 \pm 1.30	19.40 \pm 0.80	17.50 \pm 2.60	18.10 \pm 1.60	19.70 \pm 1.00	17.50 \pm 1.60	17.60 \pm 1.60	18.50 \pm 1.30	16.50 \pm 1.50	56.90 \pm 15.20	51.30 \pm 5.90	11.38 \pm 1.21
MAPE (%)	3.87 \pm 0.15	3.98 \pm 0.24	4.16 \pm 0.33	4.31 \pm 0.22	3.86 \pm 0.58	4.04 \pm 0.39	4.66 \pm 0.17	3.86 \pm 0.41	3.90 \pm 0.40	4.18 \pm 0.34	3.72 \pm 0.35	12.74 \pm 0.34	11.48 \pm 0.31	2.73 \pm 0.29
TRELLIS2														
R^2	0.07 \pm 0.12	0.11 \pm 0.13	0.08 \pm 0.12	0.02 \pm 0.15	-0.01 \pm 0.08	0.10 \pm 0.13	-0.53 \pm 0.39	0.01 \pm 0.24	-0.02 \pm 0.04	-0.17 \pm 0.21	-0.09 \pm 0.08	-0.41 \pm 0.18	0.07 \pm 0.03	0.53 \pm 0.15
MAE (kg)	16.30 \pm 3.00	16.50 \pm 2.80	16.70 \pm 2.60	16.40 \pm 2.50	16.70 \pm 2.40	16.60 \pm 2.80	16.30 \pm 2.40	32.30 \pm 28.20	30.50 \pm 24.20	17.00 \pm 0.80	16.60 \pm 1.50	48.90 \pm 35.30	40.80 \pm 12.00	11.12 \pm 2.68
MAPE (%)	3.68 \pm 0.68	3.74 \pm 0.65	3.87 \pm 0.63	3.78 \pm 0.60	3.86 \pm 0.58	3.76 \pm 0.65	3.79 \pm 0.57	7.42 \pm 6.81	6.93 \pm 5.78	4.13 \pm 0.18	3.74 \pm 0.35	10.94 \pm 7.89	9.12 \pm 2.90	2.64 \pm 0.64

body measurement model for pigs based on back point cloud data,” *Animals*, 2024.

[8] Kiyoun Kwon, Ahram Park, Hyunoh Lee, and Duhwan Mun, “Deep learning-based weight estimation using a fast-reconstructed mesh model from the point cloud of a pig,” *Computers and Electronics in Agriculture*, 2023.

[9] Chang Gwon Dang, Seung Soo Lee, Mahboob Alam, Sang Min Lee, Mi Na Park, Ha-Seung Seong, Min Ki Baek, Van Thuan Pham, Jae Gu Lee, and Seungkyu Han, “A korean cattle weight prediction approach using 3d segmentation-based feature extraction and regression machine learning from incomplete 3d shapes acquired from real farm environments,” *Agriculture*, 2023.

[10] Tsuyoshi Okayama, Yoshifumi Kubota, Atsushi Toyota, Daisuke Kohari, and Go Noguchi, “Estimating body weight of pigs from posture analysis using a depth camera,” *Animal Science Journal*, 2021.

[11] Anh H Nguyen, Jonathan P Holt, Mark T Knauer, Victoria A Abner, Edgar J Lobaton, and Sierra N Young, “Towards rapid weight assessment of finishing pigs using a handheld, mobile rgb-d camera,” *Biosystems Engineering*, 2023.

[12] Muhammad Riaz Hasib Hossain, Rafiqul Islam, Shawn R McGrath, Md Zahidul Islam, and David Lamb, “Learning-based estimation of cattle weight gain and its influencing factors,” *Computers and Electronics in Agriculture*, 2025.

[13] Charles Ruizhongtai Qi, Li Yi, Hao Su, and Leonidas J Guibas, “Pointnet++: Deep hierarchical feature learning on point sets in a metric space,” *Advances in neural information processing systems*, 2017.

[14] Rabin Dulal, Lihong Zheng, and Muhammad Ashad Kabir, “When language model guides vision: Grounding dino for cattle muzzle detection,” in *Australasian Joint Conference on Artificial Intelligence*. Springer, 2025.

[15] Rabin Dulal, Lihong Zheng, and Ashad Kabir, “Cco-maml: Efficient cattle identification using cooperative model-agnostic meta-learning,” *arXiv*, 2025.

[16] Xingyu Chen, Fu-Jen Chu, Pierre Gleize, Kevin J Liang, Alexander Sax, Hao Tang, Weiyao Wang, Michelle Guo, Thibaut Hardin, Xiang Li, et al., “Sam 3d: 3dfy anything in images,” *arXiv*, 2025.

[17] Jianfeng Xiang, Xiaoxue Chen, Sicheng Xu, Ruicheng Wang, Zelong Lv, et al., “Native and compact structured latents for 3d generation,” *arXiv preprint arXiv:2512.14692*, 2025.

[18] devinli123, “MV-SAM3D: SAM 3d objects with multi-view images,” <https://github.com/devinli123/MV-SAM3D>, Accessed: 2025-12-09.

[19] Alexey Ruchay, Vitaly Kober, Konstantin Dorofeev, Vladimir Kolpakov, and Sergei Miroshnikov, “Accurate body measurement of live cattle using three depth cameras and non-rigid 3-d shape recovery,” *Computers and Electronics in Agriculture*, 2020.

[20] Nicolas Carion, Laura Gustafson, Yuan-Ting Hu, Shoubhik Debnath, Ronghang Hu, Didac Suris, Chaitanya Ryali, Kalyan Vasudev Alwala, Haitham Khedr, Andrew Huang, et al., “Sam 3: Segment anything with concepts,” *arXiv preprint arXiv:2511.16719*, 2025.

[21] H Cantzler, “Random sample consensus (ransac),” *Institute for Perception, Action and Behaviour, Division of Informatics, University of Edinburgh*, 1981.

[22] Pierre Geurts, Damien Ernst, and Louis Wehenkel, “Extremely randomized trees,” *Machine learning*, vol. 63, no. 1, pp. 3–42, 2006.

[23] Leo Breiman, “Random forests,” *Machine learning*, vol. 45, no. 1, pp. 5–32, 2001.

[24] Dimitri P Solomatine and Durga L Shrestha, “Adaboost. rt: a boosting algorithm for regression problems,” in *2004 IEEE international joint conference on neural networks (IEEE Cat. No. 04CH37541)*. IEEE, 2004, vol. 2, pp. 1163–1168.

[25] Jerome H Friedman, “Greedy function approximation: a gradient boosting machine,” *Annals of statistics*, pp. 1189–1232, 2001.

[26] Tianqi Chen, “Xgboost: A scalable tree boosting system,” *Cornell University*, 2016.

[27] John T Hancock and Taghi M Khoshgoftaar, “Catboost for big data: an interdisciplinary review,” *Journal of big data*, vol. 7, no. 1, pp. 94, 2020.

[28] Guolin Ke, Qi Meng, Thomas Finley, Taifeng Wang, Wei Chen, Weidong Ma, Qiwei Ye, and Tie-Yan Liu, “Lightgbm: A highly efficient gradient boosting decision tree,” *Advances in neural information processing systems*, vol. 30, 2017.

[29] Sanford Weisberg, *Applied linear regression*, vol. 528, John Wiley & Sons, 2005.

[30] Arthur E Hoerl and Robert W Kennard, “Ridge regression: applications to nonorthogonal problems,” *Technometrics*, vol. 12, no. 1, pp. 69–82, 1970.

[31] Robert Tibshirani, “Regression shrinkage and selection via the lasso,” *Journal of the Royal Statistical Society Series B: Statistical Methodology*, vol. 58, no. 1, pp. 267–288, 1996.

[32] Chris Hans, “Elastic net regression modeling with the orthant normal prior,” *Journal of the American Statistical Association*, vol. 106, no. 496, pp. 1383–1393, 2011.

[33] Alex J Smola and Bernhard Schölkopf, “A tutorial on support vector regression,” *Statistics and computing*, vol. 14, no. 3, pp. 199–222, 2004.

[34] Pei-Yi Hao, “Pair- v -svr: A novel and efficient pairing nu-support vector regression algorithm,” *IEEE transactions on neural networks and learning systems*, vol. 28, no. 11, pp. 2503–2515, 2016.

[35] Oded Z Maimon and Lior Rokach, *Data mining with decision trees: theory and applications*, vol. 81, World scientific, 2014.

[36] Evelyn Fix, *Discriminatory analysis: nonparametric discrimination, consistency properties*, vol. 1, USAF school of Aviation Medicine, 1985.

[37] Peter J Huber, “Robust estimation of a location parameter,” in *Breakthroughs in statistics: Methodology and distribution*, pp. 492–518. Springer, 1992.

[38] Donald E Hilt and Donald W Seegrist, *Ridge, a computer program for calculating ridge regression estimates*, vol. 236, Department of Agriculture, Forest Service, Northeastern Forest Experiment . . ., 1977.